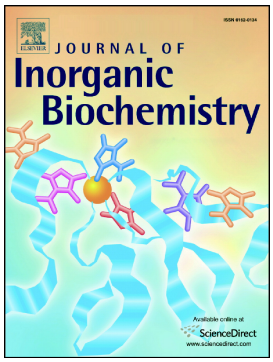

Biological activity and photocatalytic properties of a naphthyl-imidazo phenanthroline (HNAIP) ligand and its [Ir(ppy)2(HNAIP)]Cl and [Rh(ppy)2(HNAIP)]Cl complexes

Ana R. Rubio, Jairo Fidalgo, Judit Martin-Vargas, Cristina Pérez-Arnaiz, Sara R. Alonso-Torre, Tarita Biver, Gustavo Espino, Natalia Busto, Begoña García

PII: S0162-0134(19)30493-3

DOI: https://doi.org/10.1016/j.jinorgbio.2019.110885

Reference: JIB 110885

To appear in: *Journal of Inorganic Biochemistry*

Received date: 26 July 2019

Revised date: 7 October 2019

Accepted date: 7 October 2019

Please cite this article as: A.R. Rubio, J. Fidalgo, J. Martin-Vargas, et al., Biological activity and photocatalytic properties of a naphthyl-imidazo phenanthroline (HNAIP) ligand and its [Ir(ppy)2(HNAIP)]Cl and [Rh(ppy)2(HNAIP)]Cl complexes, *Journal of Inorganic Biochemistry* (2019), https://doi.org/10.1016/j.jinorgbio.2019.110885

Biological Activity and Photocatalytic Properties of a naphthyl-imidazo phenanthroline (HNAIP) ligand and its [Ir(ppy)$_2$(HNAIP)]Cl and [Rh(ppy)$_2$(HNAIP)]Cl complexes

Ana R. Rubio,[a,&] Jairo Fidalgo,[a,&] Judit Martin-Vargas,[a,&] Cristina Pérez-Arnaiz,[a] Sara R. Alonso-Torre,[b] Tarita Biver,[c] Gustavo Espino,[a*] Natalia Busto,[a*] Begoña García [a*]

[a]Departamento de Química, Universidad de Burgos, Plaza Misael Bañuelos s/n, 09001 Burgos, Spain. BG E-mail: begar@ubu.es

[b]Departamento de Biotecnología y Ciencia de los Alimentos, Universidad de Burgos, Plaza Misael Bañuelos s/n, 09001 Burgos, Spain.

[c]Dipartimento di Chimica e Chimica Industriale, Università di Pisa, Via Moruzzi 13, 56124 Pisa, Italy.

[&]JMV, JF and ARR contributed equally to this work.

In memoriam of Professor Juan Manuel Salas Peregrín and his inspiring contribution to the development of Bioinorganic Chemistry

Abstract

The synthesized 2-(hydroxy-1-naphtyl)imidazo-[4,5-f][1,10]phenantroline (**HNAIP**) ligand and its new iridium (**[Ir(ppy)$_2$(HNAIP)]Cl)** and rhodium (**[Rh(ppy)$_2$(HNAIP)]Cl)** complexes, being ppy 2-phenylpiridinate, show cytotoxic effects in SW480 (colon adenocarcinoma) and A549 (epithelial lung adenocarcinoma) cells. They all are cytotoxic in the tested cell lines; **HNAIP** and **[Rh(ppy)$_2$(HNAIP)]$^+$** are most cytotoxic, whereas **[Ir(ppy)$_2$(HNAIP)]$^+$** displays negligible cytotoxicity towards A549 cells and moderate activity towards SW480. The interaction of all three compounds with Bovine Serum Albumin (BSA), L-glutathione reduced (GSH), Nicotinamide adenine dinucleotide (NADH) and DNA was studied to explain the differences found in terms of cytotoxicity. None of them are able to interact with BSA, thus excluding bioavailability due to plasma protein interaction as the possible differentiating factor in their biological activity. By contrast, small differences have been observed regarding DNA interaction. In addition, taking advantage of the emission properties of these molecules, they have been visualized in the

cytoplasmic region of A549 cells. Inductively coupled plasma mass spectrometry (ICP-MS) experiments show, in turn, that the internalization ability follow the sequence **[Rh(ppy)$_2$(HNAIP)]$^+$** > **[Ir(ppy)$_2$(HNAIP)]$^+$** > cisplatin. Therefore, it seems clear that the cellular uptake by tumour cells is the key factor affecting the different cytotoxicity of the metal complexes and that this cellular uptake is influenced by the hydrophobicity of the studied complexes. On the other hand, preliminary catalytic experiments performed on the photo-oxidation of GSH and some amino acids such as L-methionine (Met), L-cysteine (Cys) and L-tryptophan (Trp) provide evidence for the photocatalytic activity of the Ir(III) complex in this type of reactions.

Keywords: 2-(hydroxy-1-naphtyl)imidazo-[4,5-f][1,10]phenanthroline; Iridium; Rhodium; cellular test; DNA; photo-catalysis.

Introduction

The intense work on metal complexes aimed at solving the shortcomings of current cisplatinum-like drugs and similar chemotherapeutic compounds is key to current medicinal chemistry [1–3]. Recent relevant studies are based on testing transition metal complexes other than platinum(II). As a notable instance of second generation metal-based anticancer agents, Ru(II) metal complexes such as (H_2im)[$Ru^{III}Cl_4$(DMSO)(Him)] (Him = 1H-imidazole) (NAMI-A) or trans-[tetrachlorobis(1H-indazole)ruthenate(III)] (KP1019) have reached different phases of clinical trial [4–6]. To date, other less explored transition metal ions such as gold, rhodium, iridium, iron, osmium, palladium, silver, antimony, bismuth, copper and tin have aroused increasing attention [1,7–12]. Until very recently, Rh(III) and particularly Ir(III) complexes were generally regarded as unsuitable candidates as anticancer agents owing to the typical kinetic inertness of their transition metal centres. Nowadays, due to their readily tuneable properties (attainable by changing the ancillary ligand), amphiphilic nature and relative accessibility, Ir(III) and Rh(III) complexes have become promising alternatives to platinum and ruthenium complexes [13–16]. The influence of the ligands in the biological activity of metal complexes is highly relevant; in some cases the ligand is not cytotoxic, whereas the metal complex is [14,17]. In other cases, the cytotoxicity is provided by the ligand, because the free ligand is toxic by itself [18]. However, very often the toxicity of the free ligands is

not studied in the literature [16,19,20] and the cytotoxicity is attributed to the complex. For this reason, it is advisable to study the effect of the ligand on the cytotoxicity of the metal complex; this comparison should be routine work.

Half-sandwich arene Ir(III) and Rh(III) metal complexes with diimine ligands display potent anticancer properties related to DNA intercalation [16,21,22] or perturbation of the cellular redox state [19,23,24].

Cyclometallated Ir(III) and Rh(III) complexes have been synthesized as potential diagnostic agents. Octahedral iridium(III) complexes of the type *fac*-[$IrCl_3$(DMSO)(N^N)] (N^N = bipyridine, phenanthroline, dipyridoquinoxaline, dipyrido[3,2-a:2',3'-c]phenazine or benzo[i]-dipyrido[3,2-a:2',3'-c]phenazine) are cytotoxic against lung and colon tumour cell lines, whose activity depends on the aromatic ligand and the presence of the *fac*-isomer. In spite of the aromatic ligands, DNA intercalation was not the biological mechanism of action of these complexes [25]. A similar Rhodium compound showed higher antiproliferative activity toward MCF-7 breast cancer cells compared to its Iridium analogue. Recently, studies on the properties of octahedral Rh(III) complexes of general formula [$(C^N)_2$Rh(dppz)]Cl (where C^N = 2-phenylpyridinate type ligands and dppz = dipyrido[3,2-a:2',3'-*c*]phenazine) have demonstrated that the activity depends not only on the DNA intercalator dppz, but also on the electronic and steric features of the C,N-chelating ligands [26]. Δ-[$Rh(bpy)_2$(chrysi)]$^{3+}$ (chrysi =5,6-chrysenquinonediimine) is able to intercalate into a specific region of DNA and recognize a single mismatch in a 2725 base pair plasmid [27].

It is known that the imidazole unit efficiently interacts with biomolecules and displays biological activity. Imidazo-phenanthroline-based ligands derivatives exhibit excellent light emitting efficiency [28] and attracted our attention because of their potential anticancer activity [29]. However, phenanthroimidazole derivatives exhibit poor solubility, which severely hindered their further biological application. Coordination of this scaffold to iridium(III) and rhodium(III) would lead to significant improvement in solubility.

Bearing all this in mind, the 2-(hydroxy-1-naphtyl)imidazo-[4,5-f][1,10]phenanthroline organic ligand (**HNAIP**)[30] was used to synthesize M(III) complexes denoted as **[M(HNAIP)$(ppy)_2$]$^+$** where ppy = 2-phenylpiridinate and M = Ir(III) and Rh(III) (Scheme 1). The ability of the ligand and the two

transition metal complexes synthesized to induce cellular damage was tested and their possible mode of action was studied through biosubstrates-binding tests.

Experimental

Starting materials. $RhCl_3 \cdot xH_2O$ and $IrCl_3 \cdot xH_2O$ were purchased from Johnson Mattey and used as received. The starting dimers $[Rh(ppy)_2(\mu\text{-}Cl)]_2$, and $[Ir(ppy)_2(\mu\text{-}Cl)]_2$ (ppy = 2-phenylpyridinate) were prepared according to literature procedures [31]. The HNAIP ligand was prepared according to a literature protocol [32,33]. The other reactants were purchased as follows: Phenanthroline (Alfa Aesar), glacial acetic acid (VWR), 2-hydroxy-1-naphthaldehyde (SigmaAldrich), ammonium acetate (Panreac), L-glutathione reduced (SigmaAldrich) and NADH (SigmaAldrich). CD_3SOCD_3 was obtained from Euriso-top.

Synthesis methods and characterization of complexes. All synthetic manipulations were carried out under an atmosphere of dry, oxygen-free nitrogen using standard Schlenk techniques. The solvents were dried and distilled under nitrogen atmosphere before use. Elemental analyses were performed with a Thermo Fisher Scientific EA Flash 2000 Elemental Microanalyzer. The analytical data for the new compounds were obtained from crystalline samples. The discrepancy between the calculated and the obtained values for carbon was > 0.4 %; introduction of solvent molecules in the molecular formulae improved the agreement. HR ESI (+) Mass spectra (position of the peaks in Da) were recorded with an Agilent LC-MS system (1260 Infinity LC / Quadrupole – Time of Flight Mass Spectrometry (6545 Q-TOF MS spectrometer). Dichloromethane (DCM) was used as the sample solvent and aqueous 0.1 % HCOOH/MeOH as the mobile phase. NMR samples were prepared under nitrogen atmosphere by dissolving a suitable amount of the corresponding compound in 0.5 mL of the respective oxygen-free deuterated solvent and the spectra were recorded at 298 K with a Varian Unity Inova-400 (399.94 MHz for ^1H; 100.6 MHz for ^{13}C). Typically, ^1H NMR spectra were acquired with 32 scans into 32 k data points over a spectral width of 16 ppm. ^1H and $^{13}C\{^1H\}$ chemical shifts were internally referenced to TMS via the residual ^1H and ^{13}C signals of CD_3SOCD_3 (δ = 2.50 ppm and δ = 39.52 ppm) according to the values reported by Fulmer et al.[34]. Chemical shift values (δ) are reported in ppm and coupling constants (*J*) in Hertz. The splitting of proton resonances in the reported ^1H NMR data is defined as s = singlet, d = doublet, t = triplet, m = multiplet, bs = broad singlet. 2D NMR spectra such as Correlation Spectroscopy (^1H-

^{1}H gCOSY), Nuclear Overhauser Effect Spectroscopy (^{1}H-^{1}H NOESY), were recorded using standard pulse sequences. The probe temperature (±1 K) was controlled by a standard unit calibrated with methanol as a reference. All NMR data processing were carried out using MestReNova version 10.0.2. See atom labelling for NMR peaks in Figures 1SI and 2SI in the Supporting Information.

Synthesis of (2-(hydroxy-1-naphtyl)imidazo[4,5-f][1,10]fenanthroline) (HNAIP). A mixture of 2-hydroxy-1-naphthaldehyde (0.287 g, 1.67 mmol), 1,10-phenanthroline-5,6–dione (0.25 g, 1.19 mmol), ammonium acetate (2.03 g, 26.30 mmol), and glacial acetic acid (10 mL) was refluxed for 3 h. Afterwards, the mixture was cooled down to room temperature and diluted with distilled water (40 mL approximately). Dropwise addition of concentrated aqueous ammonia to neutralize gave a yellow precipitate, which was collected and washed with water (3×10 mL). The crude product was dissolved in the minimum amount of warm ethanol and purified by crystallization. Yield: 237 mg (0.654 mmol, 55 %).

^{1}H NMR (400 MHz, DMSO-d_6, 25 °C): δ 13.75 (bs, 1H), δ 10.82 (bs, 1H), 9.05 (dd, *J* = 4.2, 1.7 Hz, 2H), 8.95 – 8.88 (m, 2H), 8.03 – 7.90 (m, 3H), 7.83 (dd, *J* = 8.1, 4.3 Hz, 2H), 7.50 – 7.44 (m, 1H), 7.39 (dd, *J* = 8.3, 2.9 Hz, 2H).

Synthesis of [Ir(ppy)$_2$(HNAIP)]Cl. In a 100 mL Schlenk flask, previously purged with nitrogen, **HNAIP** (0.020 g, 0.055 mmol) was **added** to a solution of [Ir(ppy)$_2$(μ-Cl)]$_2$ (0.029 g, 0.027 mmol) in a methanol/dichloromethane (21 mL, 4:3) mixture. The mixture was stirred overnight at 60 °C under a nitrogen atmosphere. The solution was concentrated under vacuum and a crude solid precipitated with diethyl ether (10 mL) and *n*-hexane (10 mL). Lastly, the product was filtered, washed with diethyl ether (5 mL) and dried under vacuum. *Yield:* yellow solid 0.030 g (0.033 mmol, 61 %).

M_r ($C_{45}H_{30}IrN_6OCl$) = 898.43 g/mol. Analysis Calculated for $C_{45}H_{30}ClIrN_6O\cdot(H_2O)_2$: C = 57.84 %; H = 3.67 %; N = 8.99 %; Found: C = 57.53 %; H = 3.28 %; N = 8.83 %. ^{1}H NMR (400 MHz, DMSO-d_6, 25 °C): δ 14.41 (bs, 1H, NH), δ 10.75 (bs, 1H, OH), δ 9.23 (d, *J* = 7.2 Hz, 2H, H^c), 8.28 (d, *J* = 8.2 Hz, 2H, H^3), 8.16 (d, *J* = 4.0 Hz, 2H, H^a), 8.08 (dd, *J* = 8.3, 5.1 Hz, 2H, H^b), 8.03 (d, *J* = 9.1 Hz, 1H, H$^{d/e}$), 7.99 – 7.86 (m, 6H, H^9, H^4, H$^{g/i}$, H$^{f/j}$), 7.55 (d, *J* = 5.8 Hz, 2H, H^6), 7.50-7.41 (m, 2H, H$^{e/d}$, H$^{f/j}$), 7.38 (t, *J* = 7.4 Hz, 1H, H$^{g/i}$), 7.07 (t, *J* = 7.1 Hz, 2H, H^{10}), 6.99 (m, 4H, H^5, H^{11}), 6.33 (d, *J* = 7.2 Hz, 2H, H^{12}). ^{13}C{^{1}H} NMR (101 MHz, DMSO-d_6, 25 °C): δ 166.87, 154.93, 150.51, 149.19, 148.10, 144.05, 143.93,

138.64, 133.22, 132.28, 131.70, 131.25, 130.23, 127.67, 127.22, 127.00, 125.06, 124.05, 123.84, 122.32, 119.96, 118.24, 109.85. HR ESI(+) MS (DCM): m/z (%) = 863.2108 (100) Da (m/z_{calcd} $[C_{45}H_{30}IrN_6O]^+$ = 863.2111 Da). Molar Conductivity (CH_3CN): 54.6 $S{\cdot}cm^2{\cdot}mol^{-1}$.

Synthesis of $[Rh(ppy)_2(HNAIP)]Cl$. The synthetic protocol for the Rh complex is analogous to that followed for **$[Ir(ppy)_2(HNAIP)]Cl$**. Typical amounts are: **HNAIP** (0.020 g, 0.055 mmol), $[Rh(ppy)_2Cl]_2$ (0.024 g, 0.027 mmol). Yield: yellow solid 0.023 g (0.028 mmol, 53 %).

M_r ($C_{45}H_{30}RhN_6OCl$) = 809.14 g/mol. Analysis Calculated for $C_{45}H_{30}ClRhN_6O{\cdot}(H_2O)$: C = 64.64 %; H = 3.98 %; N = 10.05 %; Found: C = 64.86 %; H = 3.55 %; N = 9.72 %. ^{1}H NMR (400 MHz, DMSO-d_6, 25 °C): δ 14.40 (bs, 1H, NH), δ 10.61 (bs, 1H, OH), δ 9.23 (d, *J* = 8.1 Hz, 2H, H^c), 8.30 (d, *J* = 8.0 Hz, 2H, H^3), 8.20 (d, *J* = 3.5 Hz, 2H, H^a), 8.10 – 7.91 (m, 9H, $2H^b$, $H^{d/e}$, $2H^9$, $2H^4$, $H^{g/i}$, $H^{f/j}$), 7.54 – 7.35 (m, 5H, H^6, $H^{e/d}$, $H^{f/j}$, $H^{g/i}$), 7.14 (t, *J* = 7.4 Hz, 2H, H^{10}), 7.05 (dd, *J* = 7.4 Hz, 4H, H^5, H^{11}), 6.34 (d, *J* = 7.7 Hz, 2H, H^{12}). $^{13}C\{^1H\}$ NMR (101 MHz, DMSO-d_6, 25 °C): δ 167.62 (d, *J* = 32.1 Hz), 164.21, 154.82, 149.11, 147.50, 143.89, 142.61, 138.78, 133.20, 132.38, 132.25, 129.96, 128.19, 127.69, 127.24, 126.63, 124.87, 124.05, 123.86, 123.26, 120.16, 118.19, 109.85. HR ESI(+) MS (DCM)**:** m/z (%) = 773.1529 Da (m/z_{calcd} $[C_{45}H_{30}RhN_6O]^+$ = 773.1536 Da). Molar Conductivity (CH_3CN): 55.5 $S{\cdot}cm^2{\cdot}mol^{-1}$.

Preparation of solutions for biological studies. For the 2-(hydroxy-1-naphtyl)imidazo-[4,5-f][1,10]phenantroline (**HNAIP**) ligand and the **$[M(ppy)_2(HNAIP)]Cl$** complexes, weighed amounts of the purified solids were dissolved in DMSO as stock solutions and maintained at 4 °C protected from light. They can be referred to as dyes/drugs and their molar concentration denoted as C_D.

Calf thymus DNA (highly polymerized lyophilized sodium salt) from Sigma-Aldrich was dissolved in water and sonicated, producing short polynucleotide fragments (ca. 1000 base pairs) according to a known procedure. The molar DNA concentration (in base pairs, ε (260 nm) = 13200 M^{-1} cm^{-1})[35] will be expressed as C_P. Bovine Serum Albumin (BSA) is supplied as crystallized and lyophilized powder (≥ 98 %, agarose gel electrophoresis and ≤0.005 % fatty acids); BSA concentration of the stock solutions was spectrophotometrically determined (ε (278 nm) = 45000 M^{-1} cm^{-1}) [36]. All other reagents were of analytical grade. The solutions were prepared with doubly distilled water from a Puranity TU System with UV lamp and ultrafilter (VWR). The aqueous solutions were

prepared using sodium cacodylate (NaCaC) as a buffer to keep the pH constant at pH = 7.0 and sodium chloride (NaCl) to adjust the ionic strength.

Cellular Assays

Cellular Visualization. To study the cellular uptake, A549 cells were seeded at a density of 5×10^3 cells per well, incubated for 24 h at 37 °C and 5 % CO_2 and then exposed to different concentrations of the studied compounds and 1 µM of Hoechst33258. After 30 minutes of incubation, the cells were visualized in a Cytation 5 Cell Imaging Multi-Mode Reader (Biotek Instruments, USA) in bright field, blue and orange fluorescence emission with a 20× objective.

MTT Assay. 1×10^4 SW480 and 5×10^3 A549 cells were cultured in 200 µL culture medium per well Dulbecco's Modified Eagle's Medium (DMEM medium), supplemented with 10 % newborn calf serum and 1 % amphotericin-penicillin-streptomycin solution in 96-well plates and incubated under 5 % CO_2 atmosphere at 37 °C. The cells were grown for 24 h and then exposed to the studied compounds. To determine cytotoxicity, the MTT (thiazolyl blue tetrazolium bromide) assay was performed. Briefly, cells were incubated for 24 h in the presence of different concentrations of the tested drugs (dissolved in DMSO). Cisplatin was used as a positive control. Then, 100 µL of 500 µg/mL of MTT was added to each well and incubated for 4 h. At the end of the incubation, the precipitated formazan product was dissolved by adding 100 µL of solubilizing solution (10 % SDS in 0.01 M HCl). The absorbance at 590 nm was read in a microplate reader (Biotek Instruments, USA). Four replicates per dose were included. The IC_{50} values calculated using the GraphPadPrism Software Inc. (v.6.01) were averaged out from at least two independent experiments.

Cellular Uptake by ICP-MS. To properly quantify the metal accumulation inside the cells, SW480 cells were seeded in culture flasks (2.5×10^6 cells in 6 mL DMEM culture medium) and incubated for 24 h at 37 °C and 5 % CO_2. After that, cells were treated for 24 h with the indicated complex concentrations, then they were harvested with trypsin and resuspended in phosphate buffered saline. The samples were digested for 24 h with 65 % HNO_3 at room temperature and then diluted with Milli-Q water to obtain 2 % HNO_3 solutions to be analyzed by inductively coupled plasma-mass spectrometry (ICP-MS).

Biophysical methods

pH measurements. To ensure near physiological conditions, the pH of all aqueous solutions was measured at 25 °C with a pH-meter fitted out with a combined glass electrode, with 3 M KCl as a liquid junction.

UV-vis absorbance and NMR spectra. Absorbance measurements were performed, to study the stability and possible aggregation processes of all three **HNAIP**, **$[Ir(ppy)_2(HNAIP)]^+$** and **$[Rh(ppy)_2(HNAIP)]^+$** under the working conditions; then, we evaluated the DNA binding and thermal stabilization, L-glutathione reduced (GSH) binding and NADH interaction. All these measurements were performed at 25 °C on a Hewlett-Packard 8453A (Agilent Technologies, Palo Alto, CA) photodiode array spectrophotometer fitted out with a Peltier temperature control system and, for GSH, on a Varian Unity Inova-400 (399.94 MHz for ^1H; 100.6 MHz for ^{13}C). DNA thermal denaturation was studied in 0.01 M buffer (NaCl and NaCaC) by heating DNA and DNA-drug solutions, from 30 to 90 °C at 0.3 °C/min scan rate, with 1 min stabilization time prior to measurements.

Photophysical measurements: Emission spectra, quantum yield and lifetime were recorded on a FLS980 Edinburgh Instrument. Emission lifetime was determinated by time-correlated single photon counting following excitation with a pulsed laser diode. Quantum yield was measured with an integrating sphere. Samples of 10^{-5} M in dry and deoxygenated DMSO and DMSO/H_2O (1:3) were prepared in quartz cuvettes and in N2 atmosphere.

Hydrophobicity (log P). The hydrophobicity of **$[Ir(ppy)_2(HNAIP)]^+$** and **$[Rh(ppy)_2(HNAIP)]^+$** was measured by the "shake flask" method between octanol/water phase partitions [37]. Octanol-saturated water and water-saturated octanol were prepared using analytical grade octanol (VWR) and double distilled water by shaking both solvents for 24 h and then to let them stand long enough to allow splitting of phases. First, the calibration curve was elaborated at 360 nm for both complexes. Then, 10 μM solutions of iridium and rhodium complex were shaken for 0.5 h in equal volume (50:50) at room temperature. After attaining equilibrium, the organic and aqueous phases were separated. Finally, metal complex concentrations were determined by UV-vis measurements at the wavelength mentioned. Partition coefficients were calculated using log P = log $[(complex)_{octanol}/(complex)_{water}]$. Triplicate experiments were performed for each complex.

Native protein electrophoresis. Native PAGE electrophoresis was carried out by incubating BSA overnight at T = 25 °C with different concentrations of the complexes in Tris HCl buffer (0.5 M, pH = 6.8) for [complex]/[protein] concentration ratios of 1, 15 and 30. After that, 5 µL of buffer sample 2× (0.01 % Bromophenol Blue and 20 % glycerol in Tris HCl buffer 0.5 M, pH 6.8) were added to 5 µL of the sample solutions and loaded onto 10 % polyacrylamide gels. Gels were run in native PAGE buffer (250 mM Tris Base, 1.92 M glycine, pH = 8.3) at 6.6 V/cm for 4 h at 4 °C to avoid thermal denaturation of the protein. Lastly, gels were stained with Coomassie brilliant blue R-250 and visualized with a Gel Doc XR+ Imaging System (Bio-Rad).

Circular dichroism (CD). CD studies were performed by adding variable amounts of drug solution to a cell containing DNA, in 0.01M buffer (NaCl and NaCaC). CD measurements were performed with a MOS-450 biological spectrophotometer (Bio-Logic SAS, Claix, France) fitted out with a 1.0 cm path-length cell.

Differential scanning calorimetry (DSC). DSC samples were prepared by adding different amounts of drug solution to different C_D/C_P (drug/DNA concentration) ratios maintaining the DMSO content at 5 % and constant DNA concentration (4×10^{-4} M). After homogenization, the samples were degassed for 30 min in a degassing station (TA Instruments, Newcastle, USA). DSC thermal denaturation studies were performed with a nanoDSC (TA Instruments, Newcastle, USA), equipped with 300 µL platinum capillary tube cells. Measurements were performed by heating the DNA and DNA/drug systems, in 0.01M buffer (NaCl and NaCaC), from 20 to 100 °C, at 1 °C/min scan rate and 3 atm pressure. The DSC curves were analyzed using the NanoAnalyze (TA Instruments, Newcastle, USA) software.

Viscosity. The viscosity assays were performed introducing 3 mL of 2×10^{-4} M DNA solution in 0.01 M buffer in a Micro-Ubbelohde viscometer (temperature control by an external thermostat – 25.0 ± 0.1 °C) and the efflux time was measured. Then, different amounts of drug solution, with DMSO as a solvent, were added and efflux times of the mixture were measured. The experiments were repeated for DNA-DMSO, and buffer-DMSO. The viscosity data were analyzed using $\eta/\eta_0 = (t - t_0)/(t_{DNA} - t_0)$, where t_0, t_{DNA} and t are the flow times for the buffer-DMSO, DNA-DMSO and DNA-drug systems, respectively, expressed as the average of at least three independent readings. Finally, relative elongation of the DNA double helix was calculated according to $L/L_0 = (\eta/\eta_0)^{1/3}$.

General procedure for the photocatalytic experiments. In a septum-capped tube we added 0.5 mL of a solution with the L-aminoacids or L-glutathione (10 mM, 0.005 mmol), the metal PC (0.01 mM – 1 % mol for L-Metionine (Met) and L-Cysteine (Cys), or 0.1 mM – 1 % mol for L-Tryptophan (Trp) and L-Glutathione (GSH) in a mixture of DMSO-d_6/D_2O (1:3 v/v for Met and Trp and 1:10 v/v for Cys) or in a mixture of MeOD/D_2O (1:3 v/v for GSH). The system was purged with O_2 until atmosphere saturation and irradiated with Blue LED light (λ= 460 nm), 24W at room temperature during 12 h. The conversion values have been calculated by ^{1}H NMR and ESI(+) MS AR.

Results and discussion

SYNTHESIS AND CHARACTERIZATION

Synthesis of Ligand. The HNAIP ligand was synthesized following a protocol from the literature which consists of reacting 2-hydroxy-1-naphthaldehyde with 1,10-phenanthroline-5,6–dione and ammonium acetate, in acetic acid as the solvent (see Scheme 1) [32,33].

Synthesis of Complexes. The new complexes of general formula [M(ppy)$_2$(N^N)]Cl (ppy = 2-phenylpyridinate, N^N = **HNAIP**; M = Ir, **[Ir(ppy)$_2$(HNAIP)]Cl** or M = Rh, **[Rh(ppy)$_2$(HNAIP)]Cl** were synthesized from the appropriate starting material [M(μ-Cl)(ppy)$_2$]$_2$ **(**M = Rh, or M = Ir) through a bridge splitting reaction in the presence of HNAIP, using a solvent mixture of dichloromethane and methanol [31,38]. The details, outlined in Scheme 1, are given in the experimental section. These complexes were isolated as pale yellow (Rh) or yellow (Ir) solids, consisting of racemic mixtures of Δ and Λ enantiomers with good yields and purities according to analytical and spectroscopic data. Moreover, they are soluble in common organic solvents such as DMSO, acetone, methanol, CH_3CN, and CH_2Cl_2 and slightly soluble in methanol/water or DMSO/water solutions.

The new derivatives were comprehensively characterized by multinuclear NMR and mass spectrometry and by elemental analysis. Assignment of the signals in the ^{1}H NMR spectra was carried out using 2D NMR experiments. (See Experimental part and Figures 1SI and 2SI for atom labelling).

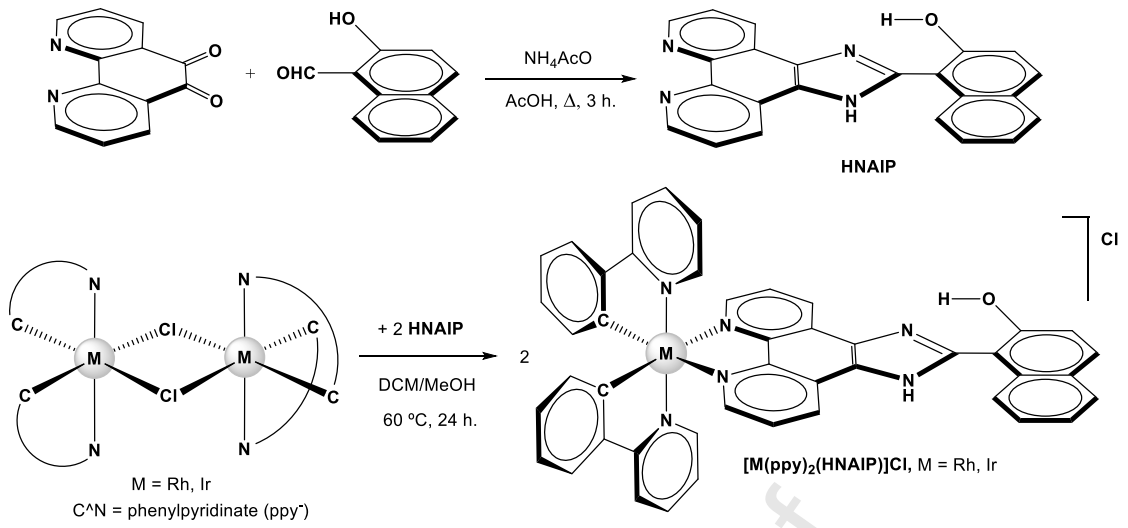

Scheme 1. Synthesis of **HNAIP** and the Rh(III) and Ir(III) complexes.

Characterization of Complexes. The ^{1}H and $^{13}C\{^{1}H\}$ NMR spectra of complexes **[Ir(ppy)$_2$(HNAIP)]$^+$** and **[Rh(ppy)$_2$(HNAIP)]$^+$** in CD_3SOCD_3 display distinctive signals for both types of ligands, i.e., **HNAIP** and ppy$^-$ (Figures 1SI and 2SI, Supporting information). These resonances are shifted compared to those of free **HNAIP** and the metal precursors with ppy$^-$, which proves the formation of the new derivatives. Moreover, the overall NMR patterns of both complexes revealed the following significant features: (a) one single set of peaks for the two equivalent 2-phenylpyridinate ligands in the ^{1}H and ^{13}C NMR spectra, consistent with the tautomeric equilibrium affecting the imidazole ring and the C_2-symmetry for the molecular structures of **[Ir(ppy)$_2$(HNAIP)]$^+$** and **[Rh(ppy)$_2$(HNAIP)]$^+$** in solution; (b) two broad singlets around 14.5 and 10.6 ppm in the ^{1}H NMR spectra of both complexes, assigned to the N-H and O-H protons, respectively; (c) Besides, in the $^{13}C\{^{1}H\}$ NMR spectra of **[Ir(ppy)$_2$(HNAIP)]Cl** and **[Rh(ppy)$_2$(HNAIP)]Cl** we ascribed respectively, the singlet at 166.9 ppm and the doublet at 167.6 ppm ($^{1}J^{103}_{Rh}$-$^{13}_{C}$ ≈ 32 Hz) to the metallated C atoms of the C^N ligands.

The HR ESI MS spectra of **[Ir(ppy)$_2$(HNAIP)]Cl** and **[Rh(ppy)$_2$(HNAIP)]Cl** display peaks whose m/z values and isotopic distribution are fully compatible with those calculated for the cationic metal complexes of formula $[M(ppy)_2(HNAIP)]^+$ (M = Ir, Rh). Molar conductivity (Λ_M) measurements conducted with solutions of complexes **[Ir(ppy)$_2$(HNAIP)]Cl** and **[Rh(ppy)$_2$(HNAIP)]Cl** in acetonitrile (10^{-3} M) were too low for 1:1 electrolytes, suggesting the presence of ion-pairs in solution stabilized through N-H---Cl interactions [39].

Stability of complexes. The stability of the compounds was also evaluated by means of absorbance measurements as a function of time. All three **HNAIP,** **[Ir(ppy)$_2$(HNAIP)]$^+$** and **[Rh(ppy)$_2$(HNAIP)]$^+$** are stable for weeks. The photostability of 10^{-2} M solutions of complexes in DMSO-d_6 and D_2O/DMSO-d_6 (3:1) was studied by ^{1}H NMR spectroscopy over a period of 24 h under irradiation (blue LED light and UV light) in an NMR tube exposed to atmospheric air. Both metal complexes are stable and do not show decomposition.

HNAIP presents an absorbance band at 330 nm, spread up to 375 nm (Figure 1A). Both complexes, **[Ir(ppy)$_2$(HNAIP)]$^+$** and **[Rh(ppy)$_2$(HNAIP)]$^+$** display intense, broad absorption bands in the UV region, attributed to spin-allowed (^{1}IL) ($^1\pi \rightarrow \pi^*$) intra ligand transitions in the cyclometallated (N^C) and (N^N) ancillary ligands. In addition, the complexes exhibit a band at about 380 nm attributed to a mixed charge transfer (CT).

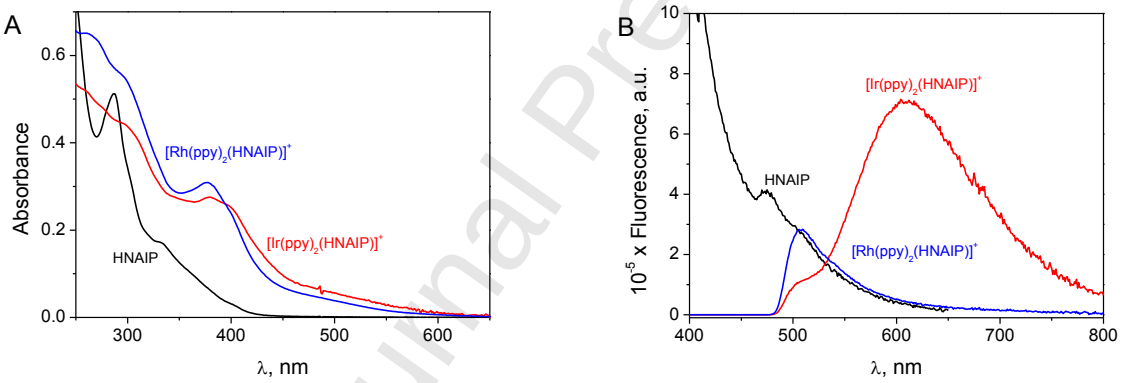

Figure 1. A) UV-Vis spectra of **HNAIP**, **[Ir(ppy)$_2$(HNAIP)]$^+$** and **[Rh(ppy)$_2$(HNAIP)]$^+$** in buffer, I = 0.01 M, pH 7.0 and T =25 °C. B) Emission spectra of **HNAIP** and complexes **[Ir(ppy)$_2$(HNAIP)]Cl** (λ_{exc} = 285 nm) and **[Rh(ppy)$_2$(HNAIP)]Cl** (λ_{exc} = 375 nm) in deoxygenated water/DMSO (3:1) (10^{-5} M) at 25 °C.

The absorbance values increased linearly with concentration (Figure 3SI); fulfillment of Lambert Beer law is observed for **HNAIP** up to 3.5×10^{-5} M with $\varepsilon_{290\,nm} = 2258$ cm^{-1}M^{-1}, for **[Ir(ppy)$_2$(HNAIP)]$^+$** up to 2.0×10^{-5} M with $\varepsilon_{380\,nm} = 12758$ cm^{-1}M^{-1} and for **[Rh(ppy)$_2$(HNAIP)]$^+$** up to 6.0×10^{-5} M with $\varepsilon_{380\,nm} = 20758$ cm^{-1}M^{-1}. Beyond these concentrations, changes in the linear profile are observed due to precipitation. Interestingly, the rhodium complex is the most soluble.

Regarding the photoluminescence properties, HNAIP displays moderate blue photoluminescence and the Ir(III) complex exhibits moderate orange photoluminescence under UV irradiation,

whereas the Rh(III) derivative shows very weak yellow photoluminescence in H_2O/DSMO. The emission spectra in deoxygenated water/DMSO (3:1) upon excitation at 285 nm for HNAIP and 375 nm for its metal complexes at room temperature are shown in Figure 1B. The emission band observed in Ir(III) complex (λ_{max} = 605 nm) is broad and unstructured, revealing a dominant contribution of the CT transitions to the emitting excited state, T_1. The photophysical data in the water/DMSO (3:1) mixture and in deoxygenated DMSO are listed in Table 1, the photoluminescent quantum yields (ϕ_{PL}) for the **[Ir(ppy)$_2$(HNAIP)]Cl** and **[Rh(ppy)$_2$(HNAIP)]Cl** derivatives are 0.57 % and <0.5 %, respectively, and the lifetimes for the excited state ($\tau_{1/2}$) are 35.6 and 6.7 ns. These features are consistent with phosphorescence as the emission mechanism for the Ir derivative [40].

Table 1. Photophysical data for 10^{-5} M of **HNAIP** ligand and its complexes **[Ir(ppy)$_2$(HNAIP)]Cl** and **[Rh(ppy)$_2$(HNAIP)]Cl** at 25 °C.

Compound	λ_{exc} (nm)	λ_{em} (nm)	ϕ_{PL} (%)	$\tau_{1/2}$ (ns)
HNAIP	285	470[a]	< 0.5[a]	4.3[a]
		450[b]	0.98[b]	4.6[b]
[Ir(ppy)$_2$(HNAIP)]Cl	375	605[a]	0.57[a]	35.6[a]
		610[b]	1.86[b]	204.1[b]
[Rh(ppy)$_2$(HNAIP)]Cl	375	510[a]	< 0.5[a]	6.7[a]
		530[b]	< 0.5[b]	1.5[b]

[a]in deoxygenated water/DMSO (3:1) and [b]in deoxygenated DMSO

CELLULAR TESTS

Cellular visualization. Since these compounds are fluorescent molecules, their visualization in A549 (epithelial lung adenocarcinoma) cells was investigated using a bioimaging microplate reader in phase contrast and blue, orange or green fluorescence emission modes. The images of A549 cells treated with either **HNAIP**, **[Ir(ppy)$_2$(HNAIP)]$^+$** or **[Rh(ppy)$_2$(HNAIP)]$^+$** during 30 min of incubation (Figure 2) show that all of them are successfully and quickly internalized by the cells. The co-staining with Hoechst33258 confirms that the metal complexes are mainly localized in the cytoplasm.

Cytotoxic Activity. Once their ability to get into cells was confirmed, MTT tests on human colon adenocarcinoma SW480 and epithelial lung adenocarcinoma A549 cells have been performed to evaluate the cytotoxic activity of **HNAIP**, **$[Ir(ppy)_2(HNAIP)]^+$** and **$[Rh(ppy)_2(HNAIP)]^+$.** The IC_{50} values are shown in Table 2. Interestingly, the metal centre exhibits a strong influence on the cytotoxicity of the synthesized complexes since the Ir(III) complex is less cytotoxic than the isoelectronic and isostructural Rh(III) complex; this complex displays almost the same cytotoxic activity than the ligand, both being more active than cisplatin. Therefore, we can conclude that not only the ligand but also the metal are key for the biological activity.

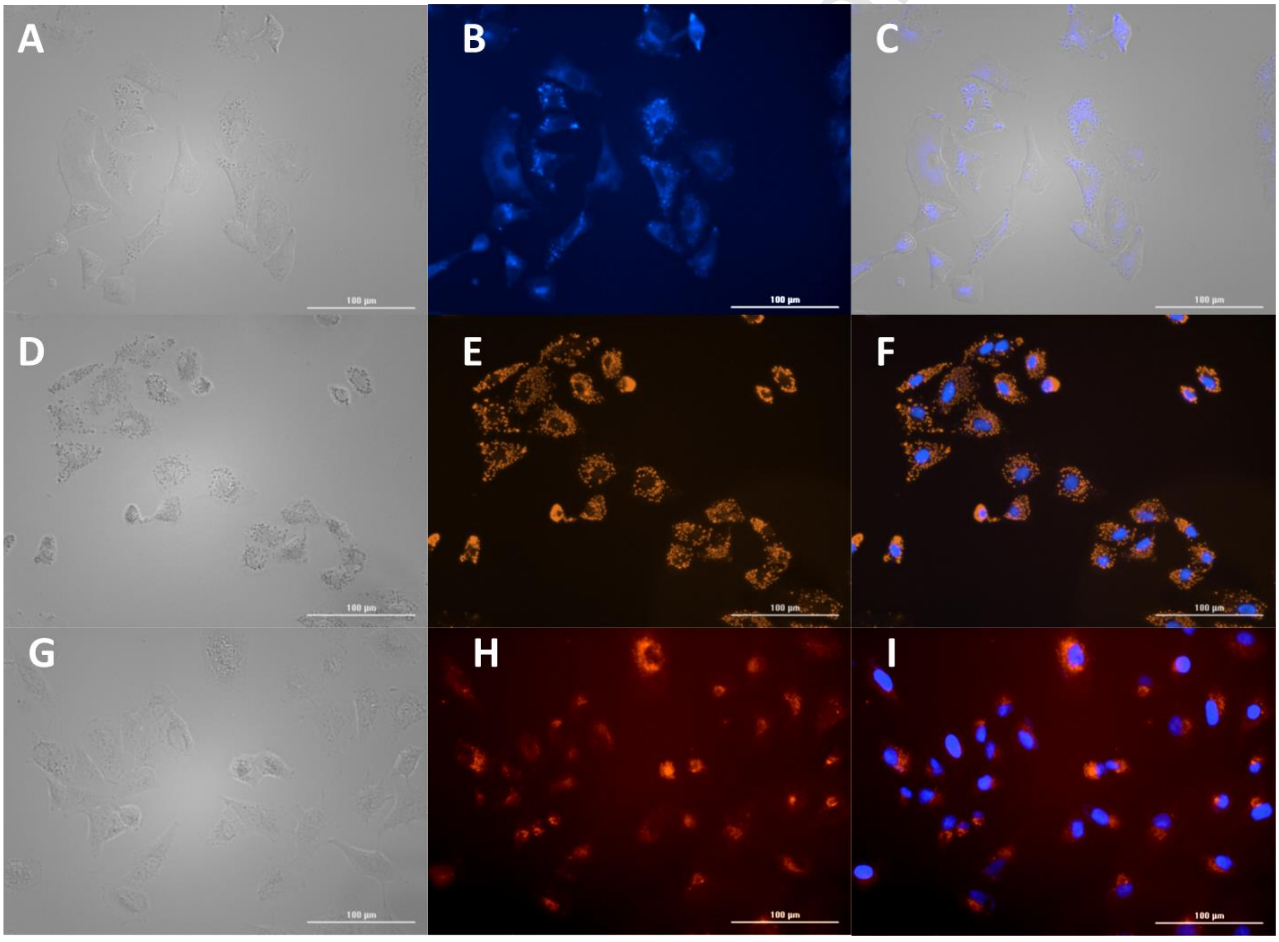

Figure 2. A549 cells treated for 30 minutes with 25 µM of the ligand **HNAIP** (1st row), 1 µM Hoechst 33258 and 10 µM of **$[Ir(ppy)_2(HNAIP)]^+$** (2nd row), 1 µM Hoechst 33258 and 25 µM of **$Rh(ppy)_2(HNAIP)]^+$** (3rd row). Bright Field (A, D and G), blue (B), orange (E and H) fluorescence emission, merged bright field and blue emission (C) and orange fluorescence emission overlapped (F and I).

Table 2. Calculated IC_{50} values of the studied compounds and the positive control, cisplatin, in SW480 (colon adenocarcinoma) and A549 (lung adenocarcinoma) cells after 24 h of exposure time.

Compound	IC_{50}, μM	
	SW480	A549
HNAIP	4 ± 1	2 ± 1
$[Rh(ppy)_2(HNAIP)]^+$	5 ± 1	9 ± 2
$[Ir(ppy)_2(HNAIP)]^+$	29 ± 2	>100
Cisplatin	39 ± 1	34 ± 1

Due to the low cytotoxicity and moderate ϕ_{PL} and $\tau_{1/2}$ values of the Ir complex (Table 1), it follows that this species could be adequate for its use in photodynamic therapy (PDT), as occurs with other Ir(III) cyclometallated complexes [41,42]. In view that the absorption bands in both complexes extend from the UV to the Vis region (Fig. 2A), these were irradiated with UV (λ= 365 nm) and Vis (λ = 460 nm) light and the IC_{50} were evaluated. Unfortunately, neither **$[Ir(ppy)_2(HNAIP)]^+$** nor **$[Rh(ppy)_2(HNAIP)]^+$** showed any IC_{50} variation upon irradiation.

Cellular uptake: Quantification by ICP-MS measurements. Since the cytotoxicity of the Rh(III) derivative differs from that of its Ir(III) analogue, a plausible explanation is searched in terms of their ability to get into cell and the cellular uptake of both complexes was quantified by ICP-MS. SW480 cells were treated for 24 h with **$[Ir(ppy)_2(HNAIP)]^+$**, **$[Rh(ppy)_2(HNAIP)]^+$** and cisplatin at C_D = 2 μM. The results show greater cell internalization of the Rh complex compared to the Ir derivative and to the well-known anticancer agent cisplatin (Figure 3). Moreover, cellular uptake and cytotoxicity usually correlate satisfactorily in other anticancer drugs described in the literature [43]. In this work, the correlation is precise, since **$[Rh(ppy)_2(HNAIP)]^+$** is approximately five-fold more cytotoxic than **$[Ir(ppy)_2(HNAIP)]^+$**, and exhibits a five-fold increase in its accumulation ability inside SW480 cells. The observed differences in the uptake of the complexes are related to the ability to cross lipid bilayers and this is often related to the partition coefficients.

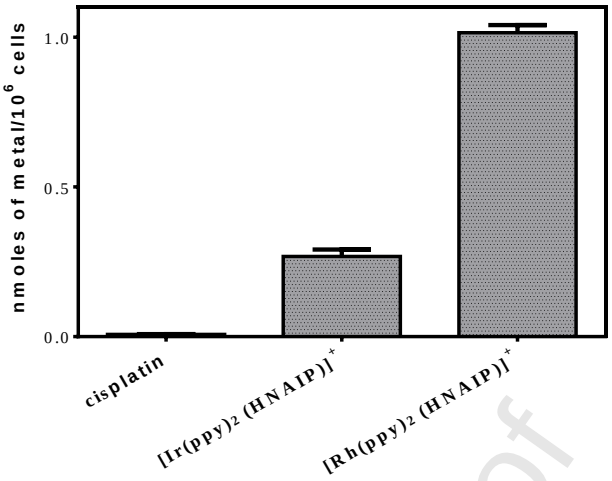

Figure 3. Metal accumulation expressed as nmoles of metal in 10^6 SW480 cells after 24 h of exposition at C_D = 2 μM.

Hydrophobicity (log P). In general, hydrophobicity is considered to play a crucial role in structure−activity relationships and in determining the biological properties of the drug [44–47]. The lipophilicity of a drug strongly affects its cellular internalization and consequently, its cytotoxic activity.

In the light of the differences observed in the cellular uptake and cytotoxicity of the complexes under study, their octanol/water partition coefficients (log P) were determined. **HNAIP** was not soluble in octanol, therefore its log P could not be obtained. The log P values for iridium and rhodium complexes were -0.11 ± 0.03 and 2.58 ± 0.08, respectively indicating greater hydrophobicity for the Rh(III) derivative compared to that of its iridium analogue. These results are consistent with cytotoxicity of the metal complexes.

BIOSUBSTRATES INTERACTION TESTS

To shed some light into the possible mode of action responsible for the obtained cytotoxicity results, the interaction of the ligand and the two organometallic complexes with several bio-targets was studied.

Interaction with BSA, GSH and NADH. Since albumin is the most abundant plasma protein, the interaction of the studied compounds with this biomolecule can easily affect their bioavailability [48]. Therefore, to verify if the differences reported above between cellular uptake of **[Ir(ppy)$_2$(HNAIP)]$^+$** and **[Rh(ppy)$_2$(HNAIP)]$^+$** could be attributed not only to their hydrophobicity but also to their interaction with serum proteins such as albumin and, consequently, to a reduction in the final drug concentration that reaches the cell, the interaction of BSA with the compounds under study was tested. We have verified by native polyacrylamide gel electrophoresis that neither the **HNAIP** ligand, nor the corresponding Ir(III) and Rh(III) complexes do interact with the protein (Figure 4SI). Therefore, the differences in terms of cytotoxicity and cellular uptake cannot be justified on the basis of the interaction with seroalbumin.

In addition, the reactivity of **[Ir(ppy)$_2$(HNAIP)]$^+$** and **[Rh(ppy)$_2$(HNAIP)]$^+$** towards GSH, overexpressed in most cancer cells, and NADH, involved in numerous enzymatic processes, were explored, since both biomolecules have been reported in the literature as adequate targets for similar metal complexes [49,50]. Therefore, UV-Vis experiments were carried out. Unfortunately, there is no binding of the metal complexes to GSH (Figure 5SI) or NADH (Figure 6SI).

Interaction with CT-DNA. The HNAIP ligand is endowed with a phenanthroline moiety. It is known that phenanthrolines essentially behave as intercalating agents between DNA nucleobases, so that they are able to cause severe structural distortions, leading to lengthening, stiffening and unwinding of the double helix [18]. On the other side, the HNAIP molecule possesses one 2-hydroxy-1-naphthyl group, which could bind to the groove by H-bonding. Transition-metal complexes containing bipyridine or phenanthroline ligands have been shown to act as groove binders or possible partial intercalators [51,52]. That is why we study here the possible interaction of both the ligand and the metal complexes with DNA. The reaction of CT-DNA with **HNAIP**, **[Ir(ppy)$_2$(HNAIP)]$^+$** and **[Rh(ppy)$_2$(HNAIP)]$^+$** can be represented by eqn 1:

$$P + D \rightleftharpoons PD \qquad (1)$$

where P stands for the polynucleotide CT-DNA, D for the drug (the ligand or metal complexes under study) and PD represents the drug/DNA complex. Henceforth, C_D and C_P denote the analytical drug and biomolecule concentration, respectively.

Circular Dichroism. CD titrations were performed by adding increasing amounts of the tested drug directly to the DNA solution. The variation of the CD spectra is somewhat modest for the ligand, but it was notable for the complexes, revealing that the metal complexes can modify the DNA structure to a greater extent than the ligand (Figure 4). The molar ellipticity in the DNA intrinsic, negative CD band (243 nm) increases as a function of the C_D/C_P ratio for all systems; this band is related to changes in the helicity of the double helix [53]. Moreover, a new band at 315 nm emerges upon increasing the concentration of the complexes, thus making evident the formation of the drug/DNA complex. The observed behaviour of **HNAIP** is compatible with binding to the groove (rather than intercalation), whereas the interaction of **$[Ir(ppy)_2(HNAIP)]^+$** and **$[Rh(ppy)_2(HNAIP)]^+$** could be compatible with partial intercalation or binding to the groove.

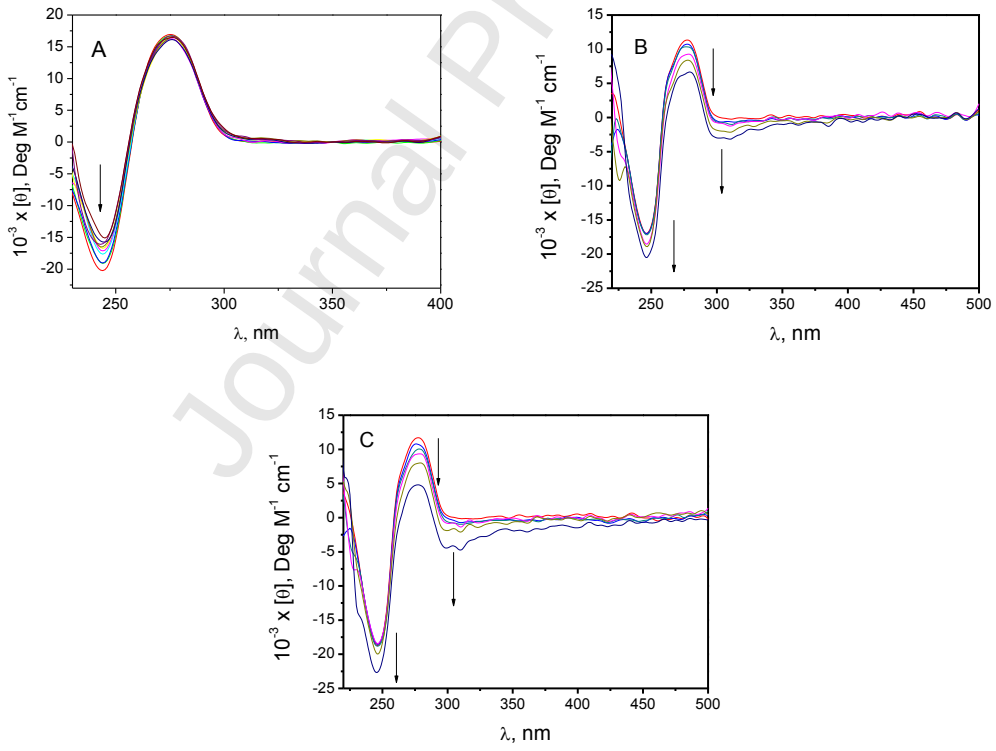

Figure 4. Circular dichroism titrations for (A) **HNAIP**/DNA, (B) **$[Ir(ppy)_2(HNAIP)]^+$**/DNA and (C) **$[Rh(ppy)_2(HNAIP)]^+$**/DNA systems; (A) C_P = 40 µM, C_D/C_P = 0 - 0.9; (B and C) C_P = 40 µM, C_D/C_P = 0 – 1.3; I = 0.01 M, pH 7.0 and 25 ˚C.

Thermal stability: UV-vis and DSC. The thermal stabilization of the DNA double helix caused by the ligand and its Ir(III) and Rh(III) complexes was studied by UV-Vis and differential scanning calorimetry (DSC). These techniques show that neither **HNAIP** nor its Ir(II) and Rh(III) derivatives stabilize the DNA double helix, since no significant variation of ΔT_m (difference between melting temperature, T_m, in the presence and in the absence of the studied compounds) was observed (Figure 7SI). This outcome points to the absence of intercalation as the mode of binding with DNA.

Viscosity. Noticeable differences in the relative elongation of DNA have been found (Figure 5). The behaviour of **HNAIP** is different (20 % contraction for $C_D/C_P \sim 0.2$) from that of **[Rh(ppy)$_2$(HNAIP)]$^+$** and **[Ir(ppy)$_2$(HNAIP)]$^+$** (no significant effect). Higher C_D/C_P ratios could not be explored due to precipitation phenomena.

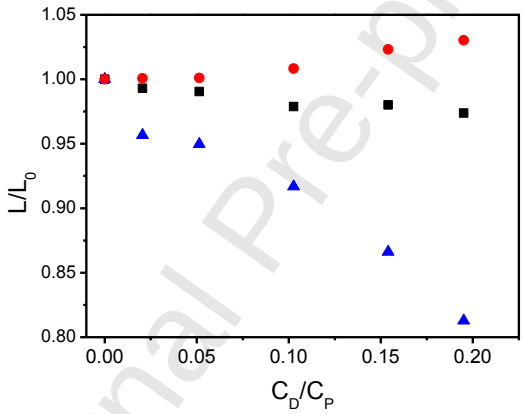

Figure 5. Relative contour length of the **HNAIP**/DNA (▲), **[Ir(ppy)$_2$(HNAIP)]$^+$**/DNA (●) and **Rh(ppy)$_2$(HNAIP)]$^+$**/DNA (▪) systems; $C_P = 2 \times 10^{-4}$ M, I = 0.01 M, pH 7.0 and 25°C.

The observed decrease in the DNA relative contour length and the absence of thermal denaturation are compatible with binding of **HNAIP** to the DNA groove by H-bonding. By contrast, the absence of significant changes in the DNA relative viscosity and melting temperature suggest external binding as the plausible binding mode for **[Rh(ppy)$_2$(HNAIP)]$^+$** and **[Ir(ppy)$_2$(HNAIP)]$^+$**. The external complex formed is favoured by the electrostatic interaction between the positive charge of the metal complex and the DNA phosphate backbone. In principle, hydrogen bonding interactions are also possible for the complexes. However, the geometry features of the complex are not adequate for this type of interaction because the cyclometallated ring prevents

accommodation of the complex in the groove and the subsequent access to the functional groups of the DNA bases.

PHOTOCATALYTIC ACTIVITY IN THE OXIDATION OF AMINO ACIDS AND PEPTIDES

L- glutathione (GSH) is overexpressed in most cancer cells where it plays a remarkable role as an antioxidant agent, preventing or mitigating oxidative stress. Proteins and enzymes, for its part, are ubiquitous and play multiple essential roles. However, Glutathione and some amino acid residues of proteins can be targets for photooxidative damage in the presence of suitable photosensitizers. On the other hand, the catalytic behavior of biscyclometallated Ir(III) complexes with 2,2'-dipyridylamine-based ligands in the photooxidation of some sulfur-containing aminoacids have been previously reported [54].

Therefore, we performed preliminary catalytic experiments on the photooxidation of L-glutathione and some amino acids like a L-methionine (Met), L-cysteine (Cys) and L-tryptophan (Trp) in the presence of **[Ir(ppy)$_2$(HNAIP)]Cl** and **[Rh(ppy)$_2$(HNAIP)]Cl** at room temperature under an O_2 atmosphere (balloon) with blue LED irradiation in DMSO-d_6/D_2O (Cys, Met, Trp) or MeOD/D_2O (GSH). Interestingly, we concluded by ^{1}H NMR that complex **[Ir(ppy)$_2$(HNAIP)]Cl** promotes the photooxidation of Met, Cys, Trp and GSH in a very efficient and selective manner after 12 h under the afore-mentioned conditions (entries 2, 5, 8, 11 in Table 3) (Figures 8SI to 10SI). The identity of the oxidized products was unambiguously established by ESI(+) MS Figures 11SI to 13SI), according to the structures shown in Figure 6. Nevertheless, the photocatlytic activity of **[Rh(ppy)$_2$(HNAIP)]Cl** in the same transformations depends strongly on the substrate, so that it is modest for Met, quantitative for Cys and GSH and null for Trp (entries 3, 6, 12 and 9 in Table 3). Control experiments in the absence of the metal photocatalysts (PC) were unproductive (entries 1, 7 and 10 in Table 3), except for cysteine which is oxidized to cystine with a yield of 44 % (entry 4 in Table 3).

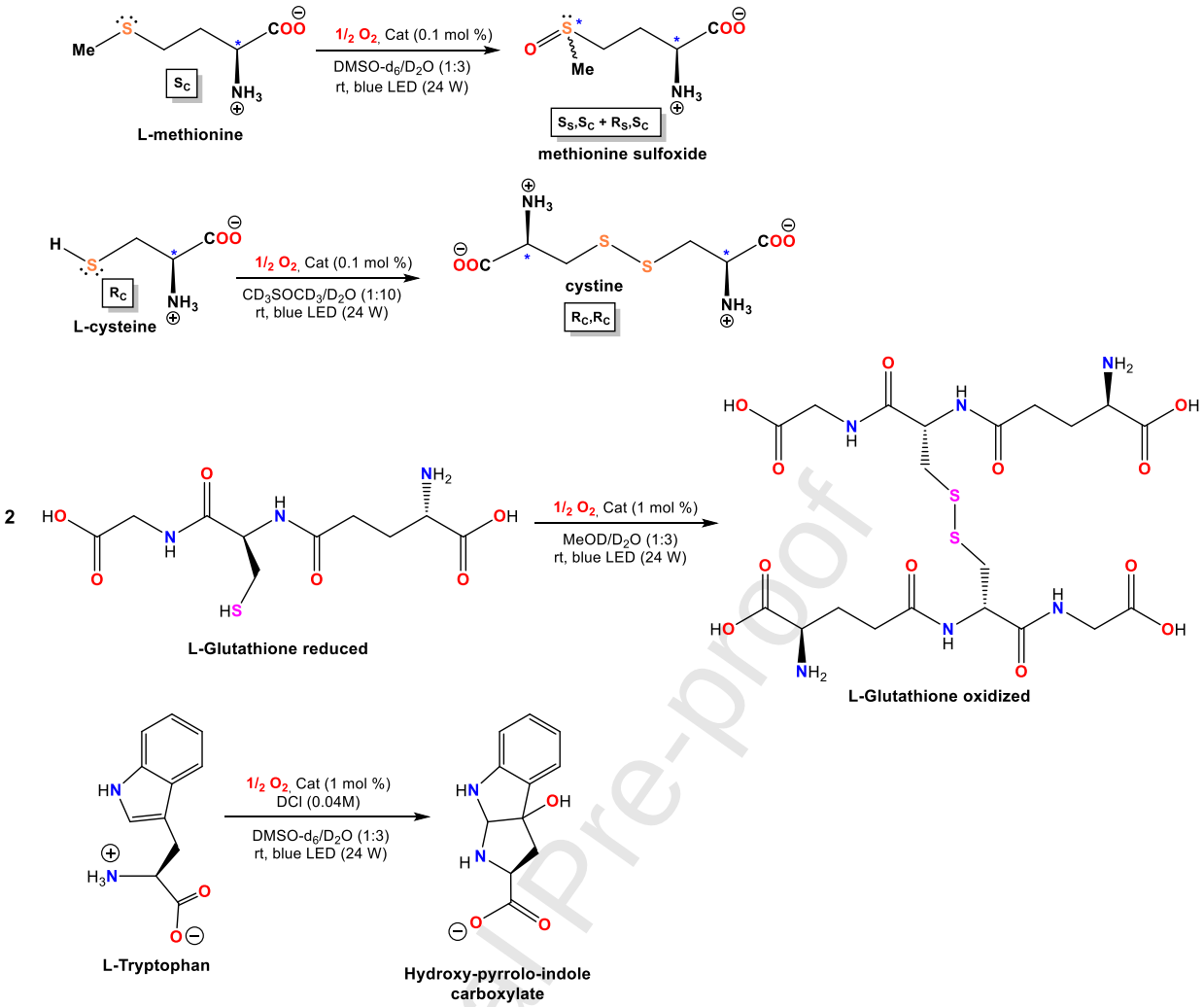

Figure 6. Reactions carried out in the presence and absence of the synthesized metal complexes **[Ir(ppy)$_2$(HNAIP)]Cl** and **[Rh(ppy)$_2$(HNAIP)]Cl**.

Table 3. Photocatalytic activity of complexes **[M(ppy)$_2$(HNAIP)]Cl (M = Rh, Ir)** in the oxidation of L-methionine, L-cysteine, L-Tryptophan and L-Glutathione under an O_2 atmosphere and blue-LED irradiation.

ENTRY	SUBSTRATE	CONDITIONS	% CONVERSION 12 H
1	L-methionine	No Cat / Blue Light / O_2	0
2	L-methionine	[Ir(ppy)$_2$(HNAIP)]Cl / Blue Light / O_2	100
3	L-methionine	[Rh(ppy)$_2$(HNAIP)]Cl / Blue Light / O_2	15
4	L-cysteine	No Cat / Blue Light / O_2	44
5	L-cysteine	[Ir(ppy)$_2$(HNAIP)]Cl / Blue Light / O_2	100
6	L-cysteine	[Rh(ppy)$_2$(HNAIP)]Cl / Blue Light / O_2	100

7	L-Tryptophan	No Cat / Blue Light / O_2	0
8	L-Tryptophan	[Ir(ppy)$_2$(HNAIP)]Cl / Blue Light / O_2	100[a]
9	L-Tryptophan	[Rh(ppy)$_2$(HNAIP)]Cl / Blue Light / O_2	0
10	L-Glutathione	No Cat / Blue Light / O_2	0
11	L-Glutathione	[Ir(ppy)$_2$(HNAIP)]Cl / Blue Light / O_2	100
12	L-Glutathione	[Rh(ppy)$_2$(HNAIP)]Cl / Blue Light / O_2	100

[a]Determined by ESI(+) MS.

Conclusions

HNAIP and the new complexes **[Ir(ppy)$_2$(HNAIP)]$^+$** and **[Rh(ppy)$_2$(HNAIP)]$^+$** have been synthesized and fully characterized. The emission properties of the three compounds under study enable their visualization in A549 epithelial lung adenocarcinoma cells after 30 minutes of incubation.

The cytotoxicity of **HNAIP** is really promising, showing the role played by the ligand in the biological activity of the complexes. Together with the ligand, the metal center plays a key role, as **[Rh(ppy)$_2$(HNAIP)]$^+$** is 6-times more cytotoxic than **[Ir(ppy)$_2$(HNAIP)]$^+$** complex in SW480 and more than 10-times in A549 cancer cells. It has been verified by ICP-MS that the cellular uptake by SW480 cells is much greater for the Rh complex than for the Ir analog due to their different hydrophobicity, and that both complexes are internalized to a greater extent than cisplatin. Moreover, the uptake values concur with the observed difference for the IC_{50} values in SW480 cells.

The interaction of all three compounds with BSA, GSH, NADH and DNA was studied. None of them is able to react with BSA, GSH and NADH and **HNAIP** can interact with DNA by binding to the groove, whereas the complexes can bind externally**.**

Regarding their behavior as photosensitizers, **[Ir(ppy)$_2$(HNAIP)]Cl** is successfully used in the aerobic catalytic photoxidation of GSH, Met, Cys and Trp.

Acknowledgements

This work was supported by "la Caixa" Banking Foundation (LCF/PR/PR12/11070003), Ministerio de Ciencia, Innovación y Universidades (RTI2018-102040-B-100), Junta de Castilla y León (BU305P18, FEDER Funds), Spain.

References

[1] Y. Cheng, Y. Qi, Current Progresses in Metal-based Anticancer Complexes as Mammalian TrxR Inhibitors., Anticancer. Agents Med. Chem. 17 (2017) 1046–1069. doi:10.2174/1871520617666170213150217.

[2] J.-X. Liang, H.-J. Zhong, G. Yang, K. Vellaisamy, D.-L. Ma, C.-H. Leung, Recent development of transition metal complexes with in vivo antitumor activity., J. Inorg. Biochem. 177 (2017) 276–286. doi:10.1016/j.jinorgbio.2017.06.002.

[3] S.H. van Rijt, P.J. Sadler, Current applications and future potential for bioinorganic chemistry in the development of anticancer drugs., Drug Discov. Today. 14 (2009) 1089–1097. doi:10.1016/j.drudis.2009.09.003.

[4] C. Riccardi, D. Musumeci, C. Irace, L. Paduano, D. Montesarchio, RuIII Complexes for Anticancer Therapy: The Importance of Being Nucleolipidic., European J. Org. Chem. 2017 (2017) 1100–1119. doi:10.1002/ejoc.201600943.

[5] A.R. Timerbaev, Role of metallomic strategies in developing ruthenium anticancer drugs., TrAC, Trends Anal. Chem. 80 (2016) 547–554. doi:10.1016/j.trac.2016.04.015.

[6] C.G. Hartinger, M.A. Jakupec, S. Zorbas-Seifried, M. Groessl, A. Egger, W. Berger, H. Zorbas, P.J. Dyson, B.K. Keppler, KP1019, a new redox-active anticancer agent - preclinical development and results of a clinical phase I study in tumor patients., Chem. Biodivers. 5 (2008) 2140–2155. doi:10.1002/cbdv.200890195.

[7] T. Marzo, D. Cirri, C. Gabbiani, T. Gamberi, F. Magherini, A. Pratesi, A. Guerri, T. Biver, F. Binacchi, M. Stefanini, A. Arcangeli, L. Messori, Auranofin, Et3PAuCl, and Et3PAuI Are Highly Cytotoxic on Colorectal Cancer Cells: A Chemical and Biological Study., ACS Med. Chem. Lett. 8 (2017) 997–1001. doi:10.1021/acsmedchemlett.7b00162.

[8] M. Singla, R. Ranjan, K. Mahiya, S.C. Mohapatra, S. Ahmad, Nitric oxide inhibition, antioxidant, and antitumour activities of novel copper(II) bis-benzimidazole diamide nanocoordination complexes., New J. Chem. 39 (2015) 4316–4327. doi:10.1039/C4NJ02147A.

[9] A. Shanmugapriya, R. Jain, D. Sabarinathan, G. Kalaiarasi, F. Dallemer, R. Prabhakaran, Structurally different mono-, bi- and trinuclear Pd(II) complexes and their DNA/protein interaction, DNA cleavage, and anti-oxidant, anti-microbial and cytotoxic studies., New J. Chem. 41 (2017) 10324–10338. doi:10.1039/C7NJ01556A.

[10] J.P.C. Coverdale, H.E. Bridgewater, J.-I. Song, N.A. Smith, N.P.E. Barry, I. Bagley, P.J. Sadler, I. Romero-Canelon, In Vivo Selectivity and Localization of Reactive Oxygen Species (ROS) Induction by Osmium Anticancer Complexes That Circumvent Platinum Resistance., J. Med. Chem. 61 (2018) 9246–9255. doi:10.1021/acs.jmedchem.8b00958.

[11] Y. Fu, A. Habtemariam, A.M. Pizarro, S.H. van Rijt, D.J. Healey, P.A. Cooper, S.D. Shnyder, G.J. Clarkson, P.J. Sadler, Organometallic Osmium Arene Complexes with Potent Cancer Cell Cytotoxicity., J. Med. Chem. 53 (2010) 8192–8196. doi:10.1021/jm100560f.

[12] S.D. Shnyder, Y. Fu, A. Habtemariam, S.H. van Rijt, P.A. Cooper, P.M. Loadman, P.J. Sadler, Anti-colorectal cancer activity of an organometallic osmium arene azopyridine complex., Medchemcomm. 2 (2011) 666–668. doi:10.1039/c1md00075f.

[13] C.-H. Leung, H.-J. Zhong, D.S.-H. Chan, D.-L. Ma, Bioactive iridium and rhodium complexes as therapeutic agents., Coord. Chem. Rev. 257 (2013) 1764–1776. doi:10.1016/j.ccr.2013.01.034.

[14] T.-S. Kang, Z. Mao, C.-T. Ng, M. Wang, W. Wang, C. Wang, S.M.-Y. Lee, Y. Wang, C.-H. Leung, D.-L. Ma, Identification of an Iridium(III)-Based Inhibitor of Tumor Necrosis Factor-α., J. Med. Chem. 59 (2016) 4026–4031. doi:10.1021/acs.jmedchem.6b00112.

[15] L. Lu, L.-J. Liu, W. Chao, H.-J. Zhong, M. Wang, X.-P. Chen, J.-J. Lu, R. Li, D.-L. Ma, C.-H. Leung, Identification of an iridium(III) complex with anti-bacterial and anti-cancer activity., Sci. Rep. 5 (2015) 14544. doi:10.1038/srep14544.

[16] G. Gupta, G. Sharma, B. Koch, S. Park, S.S. Lee, J. Kim, Syntheses, characterization and molecular structures of novel Ru(II), Rh(III) and Ir(III) complexes and their possible roles as antitumour and cytotoxic agents., New J. Chem. 37 (2013) 2573–2581. doi:10.1039/c3nj00315a.

[17] G.H. Ribeiro, L. Colina-Vegas, J.C.T. Clavijo, J. Ellena, M.R. Cominetti, A.A. Batista, Ru(II)/N-N/PPh3 complexes as potential anticancer agents against MDA-MB-231 cancer cells (N-N = diimine or diamine)., J. Inorg. Biochem. 193 (2019) 70–83. doi:10.1016/j.jinorgbio.2019.01.006.

[18] J. Valladolid, C. Hortigueela, N. Busto, G. Espino, A.M. Rodriguez, J.M. Leal, F.A. Jalon, B.R. Manzano, A. Carbayo, B. Garcia, Phenanthroline ligands are biologically more active than their corresponding ruthenium(ii) arene complexes., Dalt. Trans. 43 (2014) 2629–2645. doi:10.1039/C3DT52743C.

[19] Z. Liu, I. Romero-Canelon, B. Qamar, J.M. Hearn, A. Habtemariam, N.P.E. Barry, A.M. Pizarro, G.J. Clarkson, P.J. Sadler, The Potent Oxidant Anticancer Activity of Organoiridium Catalysts., Angew. Chemie, Int. Ed. 53 (2014) 3941–3946. doi:10.1002/anie.201311161.

[20] J.M. Zimbron, K. Passador, B. Gatin-Fraudet, C.-M. Bachelet, D. Plazuk, L.-M. Chamoreau, C. Botuha, S. Thorimbert, M. Salmain, Synthesis, Photophysical Properties, and Living Cell Imaging of Theranostic Half-Sandwich Iridium-4,4-Difluoro-4-bora-3a,4a-diaza-s-indacene (BODIPY) Dyads., Organometallics. 36 (2017) 3435–3442. doi:10.1021/acs.organomet.7b00250.

[21] S. Gencaslan, W.S. Sheldrick, Bifunctional bioorganometallic iridium(III)-platinum(II) complexes incorporating both intercalative and covalent DNA binding capabilities., Eur. J. Inorg. Chem. (2005) 3840–3849. doi:10.1002/ejic.200500223.

[22] J.M. Hearn, I. Romero-Canelon, B. Qamar, Z. Liu, I. Hands-Portman, P.J. Sadler, Organometallic Iridium(III) Anticancer Complexes with New Mechanisms of Action: NCI-60 Screening, Mitochondrial Targeting, and Apoptosis., ACS Chem. Biol. 8 (2013) 1335–1343. doi:10.1021/cb400070a.

[23] Z. Liu, I. Romero-Canelon, A. Habtemariam, G.J. Clarkson, P.J. Sadler, Potent Half-Sandwich Iridium(III) Anticancer Complexes Containing C N-Chelated and Pyridine Ligands., Organometallics. 33 (2014) 5324–5333. doi:10.1021/om500644f.

[24] L. Salassa, Polypyridyl Metal Complexes with Biological Activity., Eur. J. Inorg. Chem. 2011

(2011) 4931–4947. doi:10.1002/ejic.201100376.
[25] M. Dobroschke, Y. Geldmacher, I. Ott, M. Harlos, L. Kater, L. Wagner, R. Gust, W.S. Sheldrick, A. Prokop, Cytotoxic rhodium(III) and iridium(III) polypyridyl complexes: structure-activity relationships, antileukemic activity, and apoptosis induction., ChemMedChem. 4 (2009) 177–187. doi:10.1002/cmdc.200800311.
[26] H. Liang, T. Hao, C. Yin, X. Yang, H. Fu, X. Zheng, R. Li, D. Xiao, H. Chen, Cyclometalated Rhodium(III) Complexes Based on Substituted 2-Phenylpyridine Ligands: Synthesis, Structures, Photophysics, Electrochemistry, and DNA-Binding Properties., Eur. J. Inorg. Chem. 2017 (2017) 4149–4157. doi:10.1002/ejic.201700700.
[27] B.A. Jackson, J.K. Barton, Recognition of DNA Base Mismatches by a Rhodium Intercalator., J. Am. Chem. Soc. 119 (1997) 12986–12987. doi:10.1021/JA972489A.
[28] Y. Zhang, S.-L. Lai, Q.-X. Tong, M.-F. Lo, T.-W. Ng, M.-Y. Chan, Z.-C. Wen, J. He, J. Kc-Sham, X.-L. Tang, W.-M. Liu, C.-C. Ko, P.-F. Wang, C.-S. Lee, High Efficiency Nondoped Deep-Blue Organic Light Emitting Devices Based on Imidazole-π-triphenylamine Derivatives., Chem. Mater. 24 (2012) 61–70. doi:10.1021/cm201789u.
[29] P. Garg, U. De, N. Dehury, H.S. Kim, S. Patra, Cyclometallated imidazo-phenanthroline iridium complexes and their anticancer activity., J. Chem. Sci. (Berlin, Ger. 130 (2018) 1–8. doi:10.1007/s12039-018-1492-6.
[30] X.-Y. Wang, S. Ma, Y. He, 1-(1 H -Imidazo[4,5- f][1,10]phenanthrolin-2-yl)naphthalen-2-ol, Acta Crystallogr. Sect. E Struct. Reports Online. 67 (2011) o725–o725. doi:10.1107/S1600536811005861.
[31] S. Sprouse, K.A. King, P.J. Spellane, R.J. Watts, Photophysical effects of metal-carbon σ bonds in ortho-metalated complexes of iridium(III) and rhodium(III)., J. Am. Chem. Soc. 106 (1984) 6647–6653. doi:10.1021/ja00334a031.
[32] J.-G. Liu, B.-H. Ye, Q.-L. Zhang, X.-H. Zou, Q.-X. Zhen, X. Tian, L.-N. Ji, Enantiomeric ruthenium(II) complexes binding to DNA: binding modes and enantioselectivity., JBIC, J. Biol. Inorg. Chem. 5 (2000) 119–128. doi:10.1007/s007750050015.
[33] J.-G. Liu, B.-H. Ye, H. Li, Q.-X. Zhen, L.-N. Ji, Y.-H. Fu, Polypyridyl ruthenium(II) complexes containing intramolecular hydrogen-bond ligand: syntheses, characterization, and DNA-binding properties., J. Inorg. Biochem. 76 (1999) 265–271. doi:10.1016/S0162-0134(99)00154-3.
[34] G.R. Fulmer, A.J.M. Miller, N.H. Sherden, H.E. Gottlieb, A. Nudelman, B.M. Stoltz, J.E. Bercaw, K.I. Goldberg, NMR Chemical Shifts of Trace Impurities: Common Laboratory Solvents, Organics, and Gases in Deuterated Solvents Relevant to the Organometallic Chemist., Organometallics. 29 (2010) 2176–2179. doi:10.1021/om100106e.
[35] G. Felsenfeld, S.Z. Hirschman, A neighbor-interaction analysis of the hypochromism and spectra of DNA., J. Mol. Biol. 13 (1965) 407–427. doi:10.1016/S0022-2836(65)80106-1.
[36] S.O. Brennan, All About Albumin: Biochemistry, Genetics and Medical Applications by Theodore Peters, Jr., Trends Biochem. Sci. 21 (1996) 451–452. doi:10.1016/S0968-0004(96)80445-2.
[37] Test No. 107: Partition Coefficient (n-octanol/water): Shake Flask Method, OECD, 1995. doi:10.1787/9789264069626-en.
[38] M. Nonoyama, [Benzo[h]quinolin-10-yl-N]iridium(III) complexes., Bull. Chem. Soc. Jpn. 47 (1974) 767–768. doi:10.1246/bcsj.47.767.
[39] W.J. Geary, Use of conductivity measurements in organic solvents for the characterization of coordination compounds., Coord. Chem. Rev. 7 (1971) 81–122. doi:10.1016/S0010-

8545(00)80009-0.
[40] S. Ladouceur, E. Zysman-Colman, A Comprehensive Survey of Cationic Iridium(III) Complexes Bearing Nontraditional Ligand Chelation Motifs., Eur. J. Inorg. Chem. 2013 (2013) 2985–3007. doi:10.1002/ejic.201300171.
[41] C. Pérez-Arnaiz, M.I. Acuña, N. Busto, I. Echevarría, M. Martínez-Alonso, G. Espino, B. García, F. Domínguez, Thiabendazole-based Rh(III) and Ir(III) biscyclometallated complexes with mitochondria-targeted anticancer activity and metal-sensitive photodynamic activity, Eur. J. Med. Chem. 157 (2018) 279–293. doi:10.1016/j.ejmech.2018.07.065.
[42] M. Martinez-Alonso, N. Busto, L. Berlanga, J. V Cuevas, A. Carbayo, B. Garcia, G. Espino, L.D. Aguirre, M.C. Carrion, A.M. Rodriguez, B.R. Manzano, F.A. Jalon, E. Orti, Strong Influence of the Ancillary Ligand over the Photodynamic Anticancer Properties of Neutral Biscyclometalated Ir(III) Complexes Bearing 2-Benzoazole-Phenolates, Chemistry. (2018).
[43] M. Haghdoost, G. Golbaghi, M. Letourneau, S.A. Patten, A. Castonguay, Lipophilicity-antiproliferative activity relationship study leads to the preparation of a ruthenium(II) arene complex with considerable in vitro cytotoxicity against cancer cells and a lower in vivo toxicity in zebrafish embryos than clinically approved c, Eur. J. Med. Chem. 132 (2017) 282–293. doi:10.1016/j.ejmech.2017.03.029.
[44] S.P. Oldfield, M.D. Hall, J.A. Platts, Calculation of Lipophilicity of a Large, Diverse Dataset of Anticancer Platinum Complexes and the Relation to Cellular Uptake., J. Med. Chem. 50 (2007) 5227–5237. doi:10.1021/jm0708275.
[45] Z. Liu, L. Salassa, A. Habtemariam, A.M. Pizarro, G.J. Clarkson, P.J. Sadler, Contrasting reactivity and cancer cell cytotoxicity of isoelectronic organometallic iridium(III) complexes, Inorg. Chem. 50 (2011) 5777–5783. doi:10.1021/ic200607j.
[46] M.-G. Mendoza-Ferri, C.G. Hartinger, R.E. Eichinger, N. Stolyarova, K. Severin, M.A. Jakupec, A.A. Nazarov, B.K. Keppler, Influence of the Spacer Length on the in Vitro Anticancer Activity of Dinuclear Ruthenium-Arene Compounds., Organometallics. 27 (2008) 2405–2407. doi:10.1021/om800207t.
[47] P. Gramatica, E. Papa, M. Luini, E. Monti, M.B. Gariboldi, M. Ravera, E. Gabano, L. Gaviglio, D. Osella, Antiproliferative Pt(IV) complexes: synthesis, biological activity, and quantitative structure-activity relationship modeling., JBIC, J. Biol. Inorg. Chem. 15 (2010) 1157–1169. doi:10.1007/s00775-010-0676-4.
[48] C. Perez-Arnaiz, J. Leal, N. Busto, M.C. Carrion, A.R. Rubio, I. Ortiz, G. Barone, B. Diaz de Grenu, J. Santolaya, J.M. Leal, M. Vaquero, F.A. Jalon, B.R. Manzano, B. Garcia, Role of Seroalbumin in the Cytotoxicity of cis-Dichloro Pt(II) Complexes with (N^N)-Donor Ligands Bearing Functionalized Tails., Inorg. Chem. 57 (2018) 6124–6134. doi:10.1021/acs.inorgchem.8b00713.
[49] H. Xiang, H. Chen, H.P. Tham, S.Z.F. Phua, J.-G. Liu, Y. Zhao, Cyclometalated Iridium(III)-Complex-Based Micelles for Glutathione-Responsive Targeted Chemotherapy and Photodynamic Therapy., ACS Appl. Mater. Interfaces. 9 (2017) 27553–27562. doi:10.1021/acsami.7b09506.
[50] M. Williams, A.I. Green, J. Fernandez-Cestau, D.L. Hughes, M.A. O'Connell, M. Searcey, B. Bertrand, M. Bochmann, (CÑpzĈ)AuIII complexes of acyclic carbene ligands: synthesis and anticancer properties., Dalt. Trans. 46 (2017) 13397–13408. doi:10.1039/C7DT02804K.
[51] X.-W. Liu, J. Li, H. Li, K.-C. Zheng, H. Chao, L.-N. Ji, Synthesis, characterization, DNA-binding and photocleavage of complexes [Ru(phen)2(6-OH-dppz)]2+ and [Ru(phen)2(6-NO2-dppz)]2+., J. Inorg. Biochem. 99 (2005) 2372–2380. doi:10.1016/j.jinorgbio.2005.09.004.

[52] B.M. Zeglis, V.C. Pierre, J.K. Barton, Metallo-intercalators and metallo-insertors., Chem. Commun. (Cambridge, United Kingdom). (2007) 4565–4579. doi:10.1039/b710949k.
[53] S. Das, G.S. Kumar, Molecular aspects on the interaction of phenosafranine to deoxyribonucleic acid: Model for intercalative drug-DNA binding., J. Mol. Struct. 872 (2008) 56–63. doi:10.1016/j.molstruc.2007.02.016.
[54] M. Vaquero, A. Ruiz-Riaguas, M. Martinez-Alonso, F.A. Jalon, B.R. Manzano, A.M. Rodriguez, G. Garcia-Herbosa, A. Carbayo, B. Garcia, G. Espino, Selective Photooxidation of Sulfides Catalyzed by Bis-cyclometalated IrIII Photosensitizers Bearing 2,2'-Dipyridylamine-Based Ligands., Chem. - A Eur. J. 24 (2018) 10662–10671. doi:10.1002/chem.201801173.

Graphical Abstract

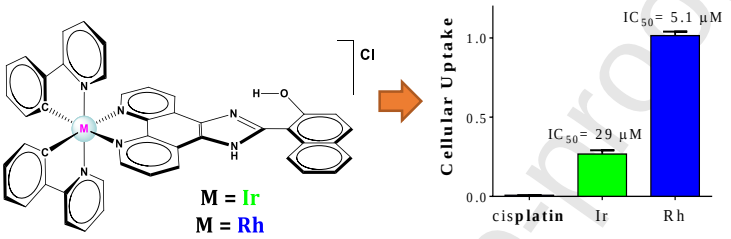

2-(hydroxy-1-naphtyl)imidazo-[4,5-f][1,10]phenanthroline ligand (**HNAIP**) used to synthesize M(III) complexes denoted as **$[M(HNAIP)(ppy)_2]^+$** where ppy = 2-phenylpiridinate and M = Ir(III) and Rh(III). Both complexes are more accumulated than cisplatin, being the cellular uptake of the Rh complex higher than that of the Ir complex which could explain their different cytotoxic activity.

Highlights

1. An imidazophenanthroline Rh complex is six times more cytotoxic than its Ir analogue.
2. The metal complexes are internalized by cells and visualized mainly in the cytoplasm
3. The Rh complex is more accumulated inside tumor cells than the Ir complex
4. Ir complex is used in the catalytic photoxidation of Glutathione, Met, Cys and Trp.